SCIENTIFIC REPORTS

OPEN

AGM2015: Antineutrino Global Map 2015

S.M. Usman[1], G.R. Jocher[2], S.T. Dye[3,4], W.F. McDonough[5] & J.G. Learned[3]

Received: 12 January 2015
Accepted: 11 August 2015
Published: 01 September 2015

Every second greater than 10^{25} antineutrinos radiate to space from Earth, shining like a faint antineutrino star. Underground antineutrino detectors have revealed the rapidly decaying fission products inside nuclear reactors, verified the long-lived radioactivity inside our planet, and informed sensitive experiments for probing fundamental physics. Mapping the anisotropic antineutrino flux and energy spectrum advance geoscience by defining the amount and distribution of radioactive power within Earth while critically evaluating competing compositional models of the planet. We present the Antineutrino Global Map 2015 (AGM2015), an experimentally informed model of Earth's surface antineutrino flux over the 0 to 11 MeV energy spectrum, along with an assessment of systematic errors. The open source AGM2015 provides fundamental predictions for experiments, assists in strategic detector placement to determine neutrino mass hierarchy, and aids in identifying undeclared nuclear reactors. We use cosmochemically and seismologically informed models of the radiogenic lithosphere/mantle combined with the estimated antineutrino flux, as measured by KamLAND and Borexino, to determine the Earth's total antineutrino luminosity at $3.4^{+2.3}_{-2.2} \times 10^{25} \overline{\nu}_e/s$. We find a dominant flux of geo-neutrinos, predict sub-equal crust and mantle contributions, with ~1% of the total flux from man-made nuclear reactors.

The neutrino was proposed by Wolfgang Pauli in 1930 to explain the continuous energy spectrum of nuclear beta rays. By Pauli's hypothesis the missing energy was carried off by a lamentably "undetectable" particle. Enrico Fermi succeeded in formulating a theory for calculating neutrino emission in tandem with a beta ray[1]. Detecting Pauli's particle required exposing many targets to an intense neutrino source. While working on the Manhattan Project in the early 1940s Fermi succeeded in producing a self-sustaining nuclear chain reaction, which by his theory was recognized to copiously produce antineutrinos. Antineutrino detection projects were staged near nuclear reactors the following decade. In 1955, Raymond Davis, Jr. found that reactor antineutrinos did not transmute chlorine to argon by the reaction: ^{37}Cl ($\overline{\nu}_e$, e^-) ^{37}Ar[2]. This result permitted the existence of Pauli's particle only if neutrinos are distinct from antineutrinos. Davis later used the chlorine reaction to detect solar neutrinos using 100,000 gallons of dry-cleaning fluid deep in the Homestake Gold Mine. Reactor antineutrinos were ultimately detected in 1956 by Clyde Cowan and Fred Reines by recording the transmutation of a free proton by the reaction ^1H ($\overline{\nu}_e$, e^+) ^1n[3,4]. This detection confirmed the existence of the neutrino and marked the advent of experimental neutrino physics.

Almost 60 years later neutrino research remains an active and fruitful pursuit in the fields of particle physics, astrophysics, and cosmology. In addition to nuclear reactors and the Sun, detected neutrino sources include particle accelerators[5], the atmosphere[6,7], core-collapse supernovae[8–11], the Earth[12,13], and most recently the cosmos[14]. We now know that neutrinos and antineutrinos have "flavor" associations with each of the charged leptons (e, μ, τ) and these associations govern their interactions. Neutrino flavors are linear combinations of neutrino mass eigenstates (ν_1, ν_2, and ν_3). This quantum mechanical phenomenon, known as neutrino oscillation, changes the probability of detecting a neutrino in a given flavor state as a function of energy and distance. Neutrino flavor oscillations along with their low cross section provide a glimpse into some of the most obscured astrophysical phenomena in the universe

[1]Exploratory Science and Technology Branch, National Geospatial-Intelligence Agency, Springfield, VA, 22150, USA. [2]Ultralytics LLC, Arlington, VA, 22203, USA. [3]Department of Physics and Astronomy, University of Hawaii, Honolulu, HI, 96822, USA. [4]Department of Natural Sciences, Hawaii Pacific University, Kaneohe, HI, 96744, USA. [5]Department of Geology, University of Maryland, College Park, MD, 20742, USA. Correspondence and requests for materials should be addressed to S.M.U. (email: Shawn.Usman@nga.mil)

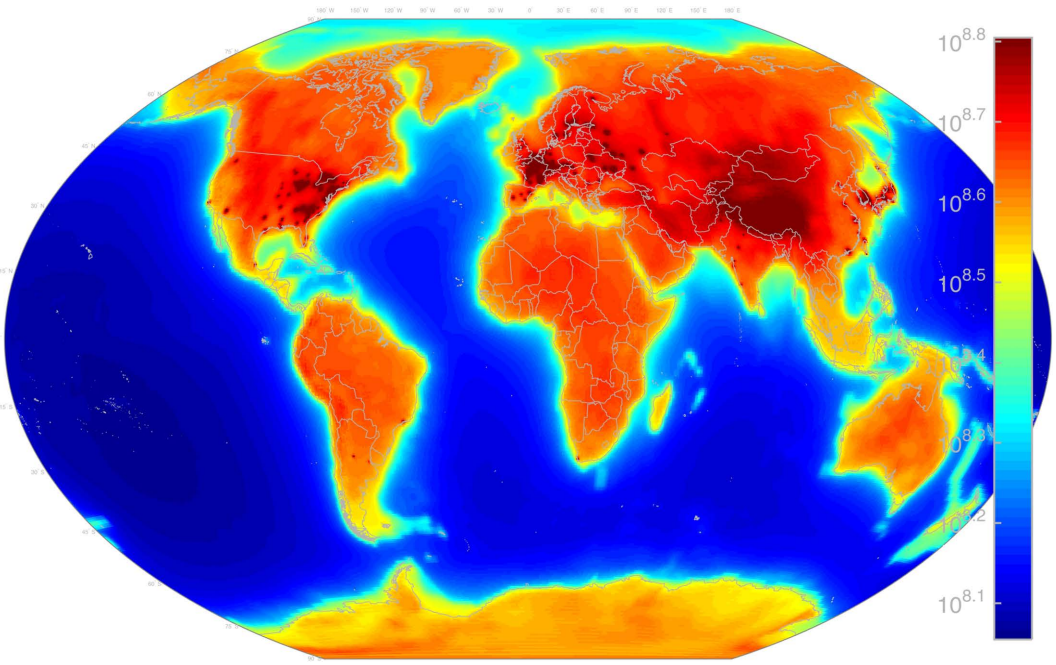

Figure 1. AGM2015: A wordlwide $\overline{\nu}_e$ flux map combining geoneutrinos from natural ^{238}U and ^{232}Th decay in the Earth's crust and mantle as well as manmade reactor-$\overline{\nu}_e$ emitted by power reactors worldwide. Flux units are $\overline{\nu}_e/\mathrm{cm}^2/\mathrm{s}$ at the Earth's surface. Map includes $\overline{\nu}_e$ of all energies. Figure created with MATLAB[45].

and most recently the otherwise inaccessible interior of our planet. Antineutrinos emanating from the interior of our planet constrain geochemical models of Earth's current radiogenic interior. Antineutrino observations of the modern Earth's interior coupled with cosmochemical analysis of chronditic meteorites from the early solar system allow scientists to model the geochemical evolution of the Earth across geologic time.

Recently, the blossoming field of neutrino geoscience, first proposed by Eder[15], has become a reality with 130 observed geoneutrino interactions[12,13] confirming Kobayashi's view of the Earth being a "neutrino star"[16]. These measurements have constrained the radiogenic heating of the Earth along with characterizing the distribution of U and Th in the crust and mantle. The development of next generation antineutrino detectors equipped with fast timing (~50 ps) multichannel plates[17] coupled with Gd/Li doped scintillator will allow for the imaging of antineutrino interactions. The imaging and subsequent reconstruction of antineutrino interactions produce directionality metrics. Directionality information can be leveraged for novel geological investigations such as the geo-neutrinographic imaging of felsic magma chambers beneath volcanos[18]. These exciting geophysical capabilities have significant overlap with the non-proliferation community where remote monitoring of antineutrinos emanating from nuclear reactors is being seriously considered[19].

Antineutrino Global Map 2015 (AGM2015) shown in Fig. 1 merges geophysical models of the Earth into a unified energy dependent map of $\overline{\nu}_e$ flux, both natural and manmade, at any point on the Earth's surface. We provide the resultant flux maps freely to the general public in a variety of formats at http://www.ultralytics.com/agm2015. AGM2015 aims to provide an opensource infrastructure to easily incorporate future neutrino observations that enhance our understanding of Earth's antineutrino flux and its impact on the geosciences. In this study we first describe the particle physics parameters used in propagating antineutrino oscillations across the planet's surface as shown in Fig. 2. A detailed description of the incorporation of anthropogenic and geophysical neutrino energy spectrum from 0–11 MeV is presented which allows for the four-dimensional generation (latitude, longitude, flux, and energy) of the antineutrino map as shown in separate energy bins in Fig. 3. A vertically stratified model of the Earth's density, shown in Fig. 4, based on seismological derived density models are combined with a cosmochemical elemental abundances to determine the geological signal of antineutrinos. This signal is then constrained by geo-neutrino measurements from KamLAND and Borexino and first order uncertainties associated with AGM map are then presented.

Neutrino Oscillations

AGM2015 incorporates the known 3-flavor oscillation behavior of antineutrinos. This starts with the standard 3-flavor Pontecorvo Maki Nakagawa Sakata (PMNS) matrix *U*:

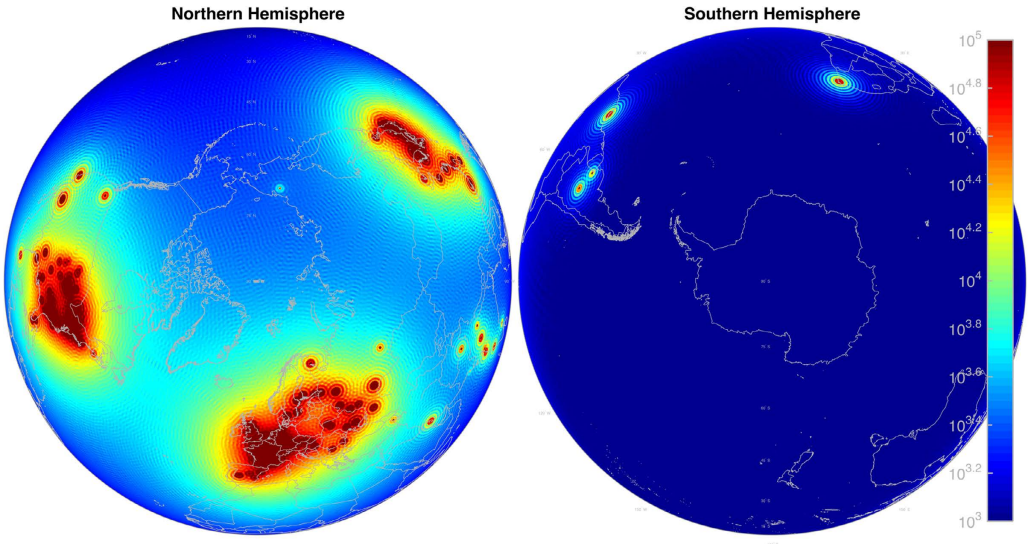

Figure 2. AGM2015 reactor-$\bar{\nu}_e$ flux in the 3.00–3.01 MeV energy bin (in logspace color). Flux units are $\bar{\nu}_e/\mathrm{cm}^2/\mathrm{s}$ at the Earth's surface. Note the visible θ_{12} oscillations at ~100 km wavelength. Figure created with MATLAB[45].

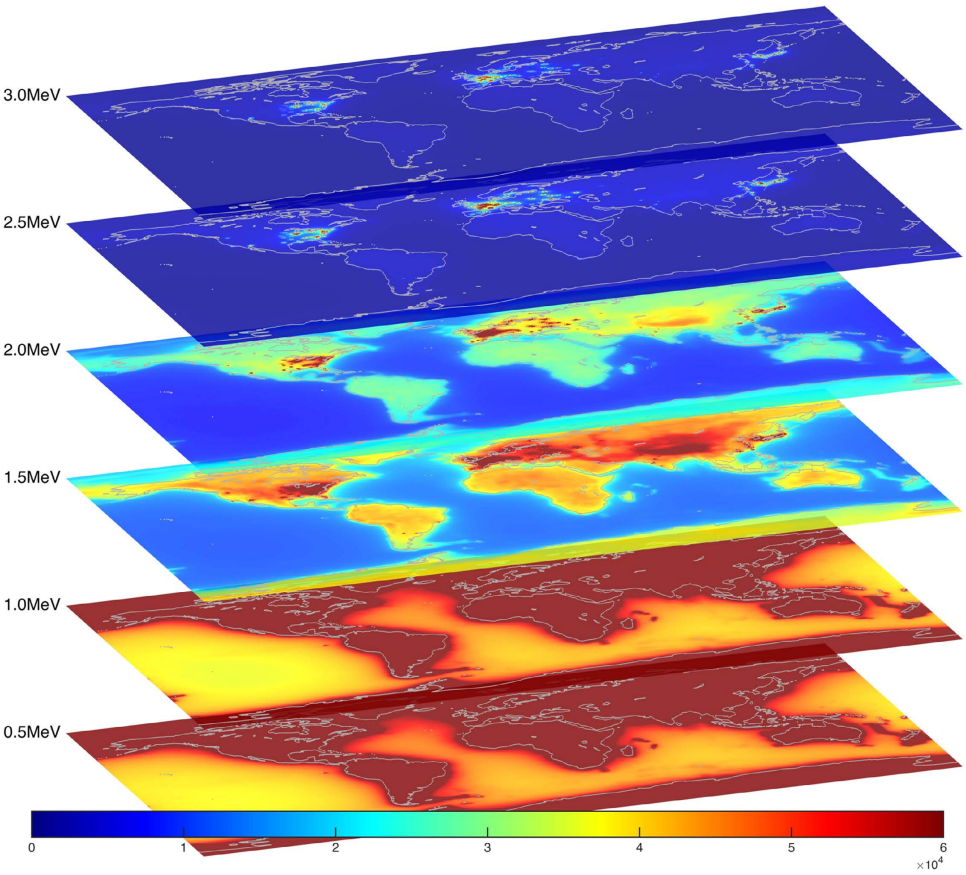

Figure 3. AGM2015 $\bar{\nu}_e$ flux ($\bar{\nu}_e/\mathrm{cm}^2/\mathrm{s}/\mathrm{keV}$) displayed at 6 select energy bins out of the 1100 total AGM2015 energy bins, which uniformly span the 0 MeV–11 MeV $\bar{\nu}_e$ energy range. Each energy bin is 10 keV wide. In conjunction with 720 longitude bins and 360 latitude bins, the highest resolution AGM2015 map is a $360 \times 720 \times 1100$ 3D matrix comprising ~300 million elements total. Figure created with MATLAB[45].

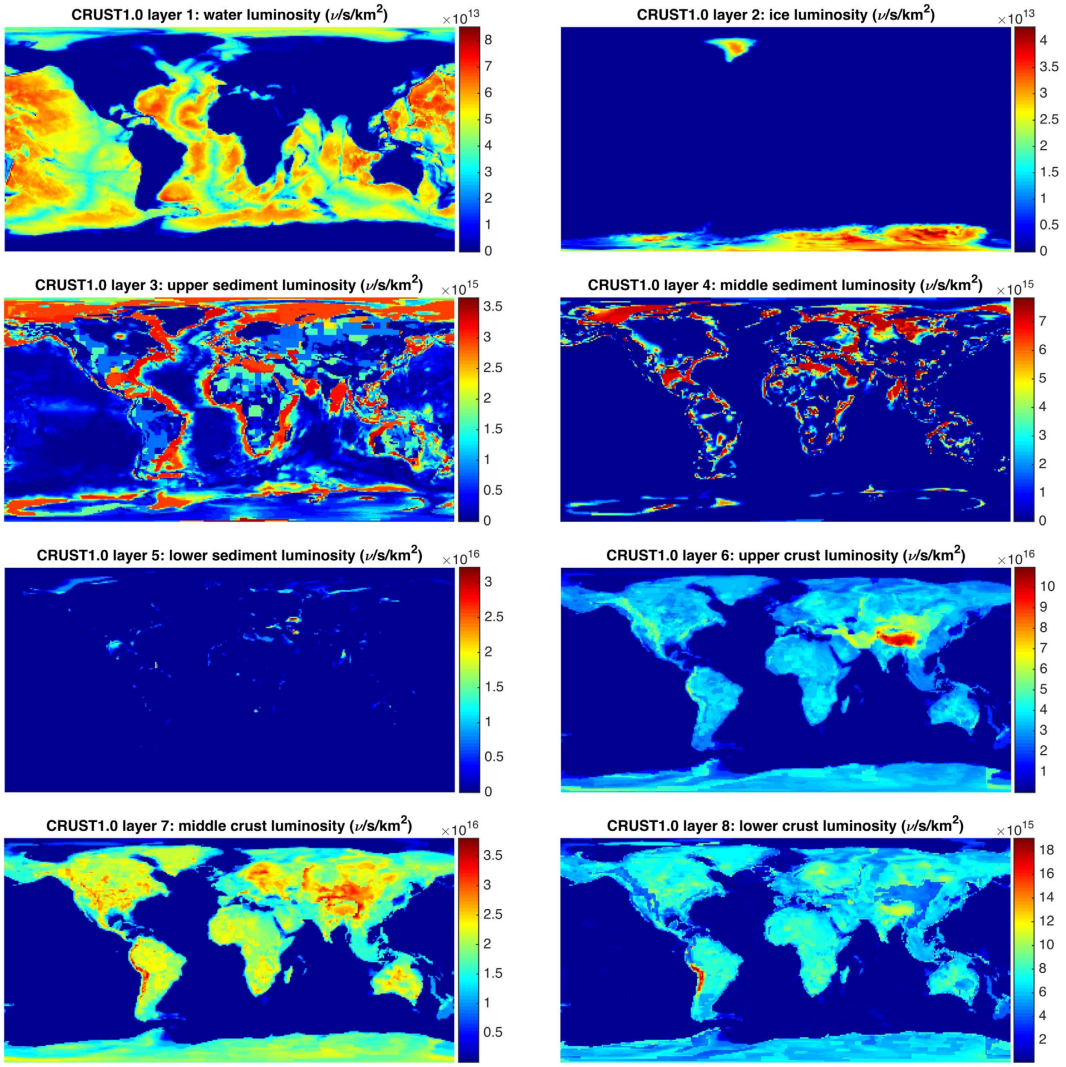

Figure 4. AGM2015 $\bar{\nu}_e$ luminosity per km^2 per CRUST1.0 layer. Each CRUST1.0 layer is composed of 180×360 1° tiles, each with a defined thickness (ranging from 0–78 km) and density (ranging from 0.9–3.4 g/cm^3). Note the layers have different colorbar scales. Figure created with MATLAB[45].

$$
\begin{aligned}
U &= \begin{pmatrix} U_{e1} & U_{e2} & U_{e3} \\ U_{\mu 1} & U_{\mu 2} & U_{\mu 3} \\ U_{\tau 1} & U_{\tau 2} & U_{\tau 3} \end{pmatrix} \\
&= \begin{pmatrix} 1 & 0 & 0 \\ 0 & c_{23} & s_{23} \\ 0 & -s_{23} & c_{23} \end{pmatrix} \begin{pmatrix} c_{13} & 0 & s_{13}e^{-i\delta} \\ 0 & 1 & 0 \\ -s_{13}e^{i\delta} & 0 & c_{13} \end{pmatrix} \begin{pmatrix} c_{12} & s_{12} & 0 \\ -s_{12} & c_{12} & 0 \\ 0 & 0 & 1 \end{pmatrix} \begin{pmatrix} 1 & 0 & 0 \\ 0 & e^{i\alpha_1/2} & 0 \\ 0 & 0 & e^{i\alpha_2/2} \end{pmatrix}
\end{aligned} \tag{1}
$$

where $c_{ij} = \cos(\theta_{ij})$ and $s_{ij} = \sin(\theta_{ij})$, and θ_{ij} denotes the neutrino oscillation angle from flavor i to flavor j in radians. In this paper we assume

$$
\begin{aligned}
\theta_{12} &= 0.587^{+0.019}_{-0.017} \\
\theta_{13} &= 0.152^{+0.007}_{-0.008}
\end{aligned} \tag{2}
$$

per a global fit by Fogli *et al.*[20] in the case of θ_{12}, and by measurements at the Day Bay experiment[21] in the case of θ_{13}. Phase factors α_1 and α_2 are nonzero only if neutrinos are Majorana particles (i.e. if neutrinos and antineutrinos are their own antiparticles), and have no influence on the oscillation survival probabilities, only on the rate of possible neutrino-less double beta decay. We assume $\alpha_1 = \alpha_2 = 0$ in this work.

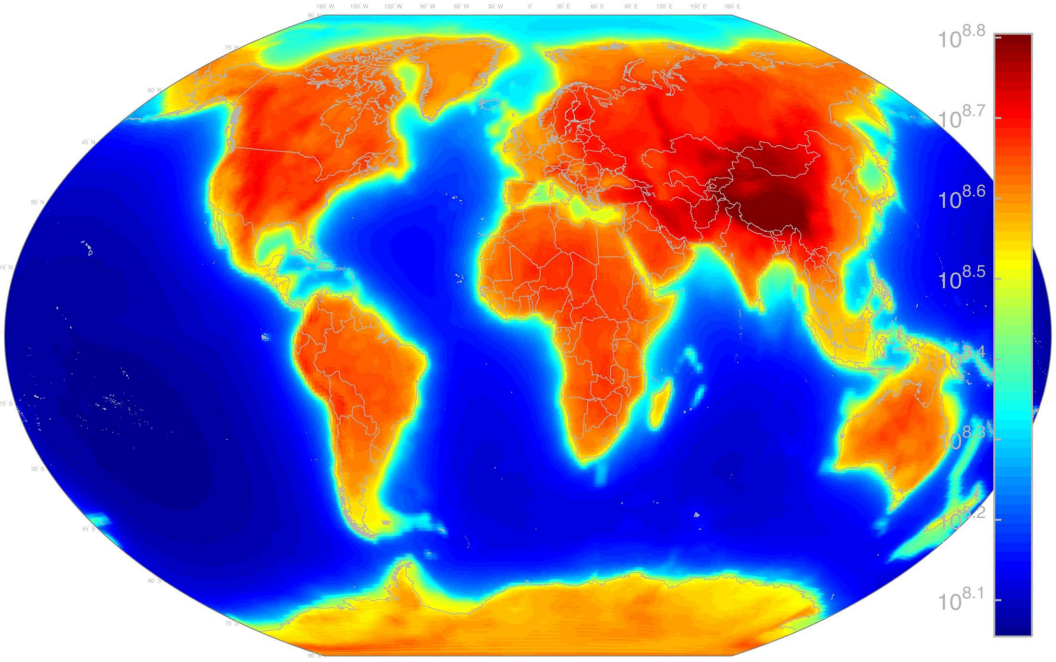

Figure 5. AGM2015 geoneutrino flux due to ^{238}U and ^{232}Th decay in the Earth's crust and mantle. Flux units are $\overline{\nu}_e/\mathrm{cm}^2/\mathrm{s}$ at the Earth's surface. Map includes $\overline{\nu}_e$ of all energies. Figure created with MATLAB[45].

We likewise assume phase factor $\delta = 0$, though this assumption may change in the future if evidence is found to support neutrino oscillations violating charge parity (CP) symmetry.

The probability of a neutrino originally of flavor α later being observed as flavor β is:

$$\begin{aligned} P_{\alpha\to\beta} &= \left|\langle\nu_\beta|\nu_\alpha(t)\rangle\right|^2 \\ &= \left|\sum_i U^*_{\alpha i} U_{\beta i} e^{-im_i^2 L/2E}\right|^2 \\ &= \delta_{\alpha\beta} - 4\sum_j\sum_{i>j}\Re\left(U^*_{\alpha i}U_{\beta i}U_{\alpha j}U^*_{\beta j}\right)\sin^2\left(\frac{\Delta m^2_{ij}L}{4E}\right) + 2\sum_j\sum_{i>j}\Im\left(U^*_{\alpha i}U_{\beta i}U_{\alpha j}U^*_{\beta j}\right)\sin^2\left(\frac{\Delta m^2_{ij}L}{4E}\right) \\ &\approx 1 - 4\sum_j\sum_{i>j}U_{\alpha i}U_{\beta i}U_{\alpha j}U_{\beta j}\sin^2\left(1.267\frac{\Delta m^2_{ij}}{\mathrm{eV}^2}\frac{L}{\mathrm{km}}\frac{\mathrm{GeV}}{E}\right) \end{aligned} \tag{3}$$

where E is the neutrino energy in GeV, L is the distance from its source the neutrino has traveled in km, and the delta-mass term $\Delta m^2_{ij} = m^2_i - m^2_j$, in eV^2. The last approximation assumes no charge parity (CP) violation ($\delta = 0$), causing the imaginary terms to fall out. The * symbol denotes a complex conjugate, and U_{ij} denotes the element of the PMNS matrix U occupying the i^{th} row and j^{th} column. Equation (3) can be employed to determine the 'survival probability' of a $\overline{\nu}_e$ of energy E GeV later being observed as the same flavor a distance L km from its source. In particular, the $P_{e\to e}$ survival probability of most interest to this paper can be expressed as Equation (4):

$$\begin{aligned} P_{e\to e} = 1 &- 4c^2_{12}c^4_{13}s^2_{12}\sin^2\left(\frac{1.27L\Delta m^2_{21}}{E}\right) - 4c^2_{12}c^2_{13}s^2_{13}\sin^2\left(\frac{1.27L\Delta m^2_{31}}{E}\right) \\ &- 4c^2_{13}s^2_{12}s^2_{13}\sin^2\left(\frac{1.27L\Delta m^2_{32}}{E}\right) \end{aligned} \tag{4}$$

For simplicity we ignore the Mikheyev-Smirnov-Wolfenstein (MSW) effect[22] on neutrinos as they travel through the Earth. We use the neutrino mixing angles and mass constants from Fogli *et al.* 2012[20] and Daya Bay 2014[21] to evaluate Equation (4) for all source-observer ranges and energies used in AGM, giving us the survival probability of seeing each source from each point in the map at each energy level. This is not a trivial task, requiring $>1\times10^{15}$ evaluations of Equation (4) for a full AGM2015 rendering. This is broken down into $\sim1\times10^6$ point sources, $\sim1\times10^6$ locations on the map at which the flux is

evaluated, and ~1×10^3 energy bins spanning the $0 < E_{\overline{\nu}_e} < 11$MeV energy range as shown in Fig. 3. Equation (4) can best be visualized in Fig. 2, which shows the θ_{12} ripples in the 3 MeV worldwide reactor-$\overline{\nu}_e$ flux.

Reactor Antineutrinos

Reactor $\overline{\nu}_e$ experiments have proven the viability of unobtrusive reactor monitoring and continue to contribute important information on neutrino properties including the possibility of additional light "sterile" neutrino flavors[23]. We use the International Atomic Energy Agency's (IAEA) Power Reactor Information System (PRIS)[24] to identify and locate 435 known man-made reactor cores in operation at the time of this writing. PRIS categorizes reactors into four states:

- Operational
- Under Construction
- Temporary Shutdown
- Permanent Shutdown

AGM2015 includes all "Operational" or "Temporary Shutdown" reactors, including many reactors in Japan affected by the Fukushima-Daiichi disaster, which are classified as "Temporary Shutdown" rather than "Permanent Shutdown." PRIS shows 435 Operational and Temporary Shutdown reactor cores distributed among 193 sites, with 870 GW_{th} total output after load factor considerations, and 72 reactor cores among 42 sites (total 156 GW_{th} at 100% load factor) currently Under Construction. The PRIS database reports thermal capacity directly, which is typically about three times electrical capacity (most reactors are about 30% efficient in converting heat into electricity). Historical "load factors" of each core are used to convert the total thermal capacity to projected current and future thermal power output. Load factors account for the down-time related to maintenance and other outages, allowing for AGM2015 to be a reliable estimate of worldwide antineutrino flux in its year of release. Typical PRIS load factors range from 70% to 90%. The 3 MeV AGM2015 reactor-$\overline{\nu}_e$ flux map due to these 435 Operational and Temporary Shutdown reactor cores is shown in Fig. 2.

The reactor-$\overline{\nu}_e$ energy spectrum assumes the shape of an exponential falloff in energy, with most reactor-$\overline{\nu}_e$ released at the lowest energies. To obtain an $\overline{\nu}_e/s/\mathrm{GW_{th}}$ reactor scaling we assume:

- The mean energy released per fission E_f is around 205 MeV[25].
- The reactor thermal power P_{th} is related to the number of fissions per second $N_f = 6.24 \times 10^{21}\, s^{-1} P_{\mathrm{th}}[\mathrm{GW}]/E_f[\mathrm{MeV}]$[25].
- $6\overline{\nu}_e$ created per fission[19]
- $2\overline{\nu}_e$ created per fission on average above the inverse beta decay (IBD) energy threshold of $E_\nu \geq 1.8$ MeV[19].

These assumptions yield $1.83 \times 10^{20}\overline{\nu}_e/\mathrm{s}/\mathrm{GW_{th}}$ (of all energies) emitted from a reactor, with $0.61 \times 10^{20}\overline{\nu}_e/\mathrm{s}/\mathrm{GW_{th}}$ emitted above the 1.8 MeV IBD detection threshold. This is a mean value representative of a typical pressurized water reactor at the beginning of its fuel cycle[19]. We find the summed worldwide reactor power output to be 870 GW_{th}, and the resultant $\overline{\nu}_e$ luminosity to be $1.6 \times 10^{23}\overline{\nu}_e/s$ and 0.04 TW. Jocher *et al.*[26] is recommended for a deeper discussion of reactor-$\overline{\nu}_e$ detection via IBD detectors.

Geoneutrinos

Observations from geology, geophysics, geochemistry, and meteoritics allow for a range of non-unique solutions for the composition of the Earth. The relative proportion of Fe, O, Mg, and Si in chondritic meteorites individually varies by ~15% each and reflects spatial and temporal differences in where these rocks formed in the early solar nebula. Likewise, refractory elements have 25% variation in their relative abundance, which translates into a factor of two in absolute concentration difference of these elements. Even greater enrichment factors of these elements occur when the volatile inventory (e.g., H_2O, CO_2, N_2) is mostly lost, as during terrestrial planet assembly. Finally, because the Earth's core is taken to have negligible amounts of Th, U and K[27–29], due to their limited solubility in core-forming metallic liquids, this becomes another 50% enrichment factor in the radiogenic elements in the silicate Earth. Consequently, compositional models predict between 10 and 30 ng/g U (and Th/U = 3.9, the chondritic ratio) for the silicate Earth. Given the planetary ratio of Th/U and K/U (1.4×10^4)[30], and the absolute U content of the silicate Earth, its heat production for a 10 ng/g U model roughly corresponds to a surface heat flow of 10 TW and likewise 30 ng/g U to ~30 TW. Estimates of the Earth's radiogenic heat production thus vary from low power models (10–15 TW of power from K, Th, and U), through medium power models (17–22 TW), and to high power models (>25 TW)[31]. Accordingly, detecting the Earth's flux of geoneutrinos can provide crucial data to test competing theories of the bulk Earth.

Two observatories, one in Japan (KamLAND) and one in Italy (Borexino), are making ongoing measurements of the surface flux of geoneutrinos at energies above the IBD threshold energy $E_\nu \geq 1.8$ MeV.

		U (10^{-6})	Th (10^{-6})	K (10^{-2})
	H_2O[32]	0.0032	0	0.04
	Sediment[36]	1.73 ± 0.09	8.10 ± 0.59	1.83 ± 0.12
	Upper Crust[36]	2.7 ± 0.6	10.5 ± 1.0	2.32 ± 0.19
CC	Middle Crust[36]	$0.97^{+0.58}_{-0.36}$	$4.86^{+4.30}_{-2.25}$	$1.52^{+0.81}_{-0.52}$
	Lower Crust[36]	$0.16^{+0.14}_{-0.07}$	$0.96^{+1.18}_{-0.51}$	$0.65^{+0.34}_{-0.22}$
OC	Crust[36]	0.07 ± 0.02	0.21 ± 0.06	0.07 ± 0.02
	LM[36]	$0.3^{+0.05}_{-0.02}$	$0.15^{+0.28}_{-0.10}$	$0.03^{+0.04}_{-0.02}$
	Mantle[12,13,30,36]	0.011 ± 0.009	0.022 ± 0.040	0.015 ± 0.013
		^{238}U	^{232}Th	^{40}K
	Isotope abundance	0.99275	1.0	0.000117
	Lifetime (Gyr)[48,49]	6.4460	20.212	1.8005
	Multiplicity ($\overline{\nu}_e$/decay)	6	4	0.893
	Mass (amu)	238.05	232.04	39.964

Table 1. AGM2015 distribution and properties of U, Th, and K, which are the main emitters of electron antineutrinos. Abundances in the various stratified crustal layers are shown at the top of the table, including Oceanic Crust (OC), Continental Crust (CC), and Lithospheric Mantle (LM). Relevant isotopic properties are presented at the bottom of the table. Note the abundances are unit-less fractions. Uncertainties shown in this table derived from Huang *et al.*[36], Arevalo *et al.*[30], Gando *et al.*[12], and Bellini *et al.*[13].

	L ($10^{25}\overline{\nu}_e$/s)				
	^{238}U	^{232}Th	^{40}K	Reactors	$\Sigma_{U,Th,K,Reactors}$
Crust	$0.21^{+0.065}_{-0.050}$	$0.19^{+0.073}_{-0.042}$	$0.91^{+0.22}_{-0.17}$	–	$1.3^{+0.36}_{-0.26}$
Mantle	0.32 ± 0.28	0.14 ± 0.26	1.6 ± 1.4	–	2.1 ± 1.9
$\Sigma_{Crust,\ Mantle}$	$0.53^{+0.34}_{-0.33}$	$0.33^{+0.33}_{-0.30}$	$2.5^{+1.6}_{-1.6}$	$0.016^{+0.001}_{-0.001}$	$3.4^{+2.3}_{-2.2}$

Table 2. Contribution of geoneutrino luminosities L in AGM2015 for ^{238}U, ^{232}Th, and ^{40}K $\overline{\nu}_e$ emitted by the Earth. The reactor-$\overline{\nu}_e$ luminosity is $1.6 \pm 0.1 \times 10^{23}\overline{\nu}_e/s$ and 40 GW for the world's 435 reactor cores, which together output 870GW_{th}[24]. Uncertainties shown in this table derived from Huang *et al.*[36], Arevalo *et al.*[30], Gando *et al.*[12], and Bellini *et al.*[13].

At Japan the flux measurement is $(3.4 \pm 0.8) \times 10^6\,cm^{-2}\ s^{-1}$ [12], while at Italy the flux measurement is $(4.3 \pm 1.3) \times 10^6\,cm^{-2}\ s^{-1}$ [13]. Note that it is sometimes convenient to express geoneutrino flux as a rate of recorded interactions in a perfect detector with a given exposure using the Terrestrial Neutrino Unit (TNU)[32], however in this work we focus on simple $\overline{\nu}_e$ flux ($\overline{\nu}_e/cm^2/s$) and luminosity ($\overline{\nu}_e/s$).

AGM models the Earth as a 3D point cloud consisting of roughly 1 million points. National Oceanic and Atmospheric Administration (NOAA) Earth TOPOgraphical 1 (ETOPO1) "ice" data[33] is used to provide worldwide elevations with respect to the World Geodetic System 84 (WGS84) ellipsoid. Zero-tide ocean surface corrections to the WGS84 ellipsoid were obtained from the National Geospatial-Intelligence Agency (NGA) Earth Gravitational Model 2008[34] (EGM2008) for modeling the ocean surface elevations around the world. Underneath these surface elevations we model 8 separate crust layers using CRUST 1.0[35], shown in Fig. 4, as well as a 9th adjoining layer per Huang *et al.*[36] which reaches down to the spherical mantle, creating a seamless earth model. Certain crust tiles which are too large (about 200 km across at the equator) to be adequately modeled as point sources are instead modeled as collections of smaller tiles using numerical integration, which recursively subdivides large tiles into progressively smaller sub-tiles until the contribution of each is less than 0.001 TNU.

Geoneutrino flux is produced from the decay of naturally occurring radioisotopes in the mantle and crust: ^{238}U, ^{232}Th, ^{235}U, ^{40}K, ^{87}Rb, ^{113}Cd, ^{115}In, ^{138}La, ^{176}Lu, and ^{187}Re[37]. However, we only consider ^{238}U and ^{232}Th in our flux maps as all other elements' energy spectrum is considerably below the IBD energy threshold of $E_\nu \geq 1.8$ MeV. All abundances for the crust and mantle can be seen in Table 1. As shown in Table 2, K is the largest contributor to $\overline{\nu}_e$ luminosity but its energy is below the IBD threshold. All elements other than U, Th, and K have a negligible contribution to the Earth's $\overline{\nu}_e$ luminosity.

Successful detection of $\overline{\nu}_e$ below 1.8 MeV remains elusive; if successful the incorporation of the remaining radioisotopes would be beneficial to future versions of AGM. The Earth's core was assumed to have no significant contribution to the $\overline{\nu}_e$ flux due to limiting evidence for a georeactor[38] and no

	L ($10^{25}\overline{\nu}_e$/s) > 1.8 MeV				
	^{238}U	^{232}Th	^{40}K	Reactors	$\Sigma_{U,Th,K,Reactors}$
fraction > 1.8 MeV	0.068	0.042	0.0	0.35	–
Crust	$0.014^{+0.0044}_{-0.0034}$	$0.0082^{+0.0031}_{-0.0018}$	0.0	–	$0.022^{+0.0075}_{-0.0052}$
Mantle	0.021 ± 0.019	0.0059 ± 0.011	0.0	–	0.027 ± 0.030
$\Sigma_{Crust,\ Mantle}$	$0.035^{+0.023}_{-0.022}$	$0.014^{+0.014}_{-0.013}$	0.0	$0.006^{+0.001}_{-0.001}$	$0.055^{+0.037}_{-0.035}$

Table 3. Contribution of geoneutrino luminosities L in AGM2015 above the IBD threshold $E_\nu \geq 1.8$ MeV for ^{238}U, ^{232}Th, and ^{40}K $\overline{\nu}_e$ emitted by the Earth. The reactor-$\overline{\nu}_e$ luminosity $\geq$1.8 MeV is $0.6 \pm 0.1 \times 10^{23}\overline{\nu}_e/s$ and 26 GW for the world's 435 reactor cores, which together output 870 GW_{th}[24]. Uncertainties shown in this table derived from Huang *et al.*[36], Arevalo *et al.*[30], Gando *et al.*[12], and Bellini *et al.*[13].

Δm^2_{12}[20]	$7.54^{+0.21}_{-0.18} \times 10^{-5}$ eV^2
Δm^2_{13}[21]	$2.59^{+0.19}_{-0.20} \times 10^{-3}$ eV^2
$\sin^2\theta_{12}$[20]	$0.307^{+0.017}_{-0.016}$
$\sin^2\theta_{13}$[21]	$0.02303^{+0.00210}_{-0.00235}$
steady-state $\overline{\nu}_e$ survival fraction[20,21]	0.549 ± 0.012
Reactor $\overline{\nu}_e$/fission[21,25]	6.00 ± 0.18
Reactor Energy[MeV]/fission[25,47]	205 ± 1
Reactor $\overline{\nu}_e$/fission > 1.8 MeV[21,25]	2.100 ± 0.013

Table 4. AGM2015 reactor-$\overline{\nu}_e$ parameters and $\overline{\nu}_e$ oscillation parameters. θ_{12} oscillation parameters from Fogli *et al.*[20], and θ_{13} oscillation parameters from results of the Daya Bay[21] $\overline{\nu}_e$ experiment.

appreciable amount of ^{238}U, ^{232}Th, or ^{40}K isotopes[27]. While certain core models support upper limits of K content at the ~100 ppm level[28], which would be sufficient for up to ~1–2 TW of radiogenic heating in the present day, "constraints on K content are very weak"[29], and in the absence of stronger evidence we've chosen to assume a K-free core.

Mantle abundances were derived from empirical geo-neutrino measurements at KamLAND[12] and Borexino[13]. We deconstructed the reported geo-neutrino flux from each observation into separate contributions from U and Th according to a Th/U ratio of 3.9. From each of these, we subtracted the predicted crust flux contributions[36] at each observatory, averaging the asymmetric non-gaussian errors, to arrive at estimates of the mantle contributions. We then combined the estimates of the mantle U flux and the mantle Th flux contributions from each observation in a weighted average. The resulting best estimates for the mantle U and Th flux contributions were finally converted to homogeneously distributed mantle abundances using the spherically symmetric density profile of the Preliminary Reference Earth Model (PREM)[39] along with a corresponding correction to account for neutrino oscillations. Corresponding values for K were found by applying a K/U ratio of $13{,}800 \pm 1300$[30]. The resulting AGM2015 U, Th and K mantle abundances are presented in Table 1. The main sources of uncertainty in these estimates are the observational errors in the flux measurements and limited knowledge of the subtracted crust fluxes. A detailed description of the methods and relevant conversion factors used here are presented in Dye[31].

AGM2015 neutrino luminosities are for total numbers of neutrinos. Although almost all are originally emitted as electron antineutrinos, on average only ~0.55 of the total remain so due to neutrino oscillations. We calculate the total Earth $\overline{\nu}_e$ luminosity to be $3.4^{+2.3}_{-2.2} \times 10^{25}$ $\overline{\nu}_e$ s^{-1}. A detailed breakdown of ^{238}U, ^{232}Th, and ^{40}K geoneutrino luminosity from the lithosphere and mantle can be seen in Table 2 (for all energies), as well as in Table 3 for $E_\nu \geq 1.8$ MeV. Figure 5 shows the combined AGM2015 crust + mantle $\overline{\nu}_e$ flux.

Uncertainty

The underlying interior structure and composition of the Earth is, in some regards, still poorly understood. The concentration and distribution of radioisotopes, whose decay chains produce geoneutrino flux, dominate the uncertainties. Therefore modeling of the distribution, energy spectra, and total flux of geoneutrinos remains a challenging task on its own. A full description of the uncertainty in each element of the AGM flux maps is not available at this time, however, we have defined the uncertainties in the

specific building blocks of the AGM in Tables 1 and 4 as well as the systematic uncertainties present in the various geoneutrino luminosity categories in Tables 2 and 3. The uncertainties in Tables 1 and 4 in particular can be used to create Monte Carlo instances of the AGM flux maps, which could be used to evaluate the variances in each element of the AGM flux map, as well as co-variances between map elements. Such a full-scale Monte Carlo covariance matrix is impractical, however, due to the large number of map elements, ~300 Million, which would end up producing a 300 Million × 300 Million full-size covariance matrix.

In most parts of the AGM2015 map uncertainties are strongly correlated over space and energy. This is due to the fact that the greatest uncertainty lies in ingredients that affect all map elements nearly equally, such as elemental abundances in the Earth's crust and mantle. Other ingredients which might introduce more independent uncertainty, such as the volume or density of specific crust tiles, are much more likely to introduce minimal correlations, or only slight regional correlations. Since reactor-$\overline{\nu}_e$ flux is generally better predicted than geo-$\overline{\nu}_e$ flux, and since near a core the reactor-$\overline{\nu}_e$ flux will dominate the overall $\overline{\nu}_e$ flux, we would expect smaller fractional uncertainties near reactors than in other regions of the world.

We attempt to apply systematic uncertainties to AGM2015 where appropriate, and to derive these uncertainties from previous work in the field where possible rather than reinvent the wheel. For our uncertainty models we turn to Huang *et al.*[36] and Dye[31]. Doing so allows us to apply systematic uncertainties to the various $\overline{\nu}_e$ source categories in Tables 2 and 3 while avoiding the significant computational burden of a full Monte Carlo analysis, as well as the questions that would arise afterward of how to describe the various levels of regional correlation in flux uncertainty across space and energy.

Conclusion

Electron antineutrino measurements have allowed for the direct assessment of 7–29 TW[31] power from U and Th along with constraining a geo-reactor <3.7 TW at the 95% confidence level[12]. Such measurements promise the fine-tuning of BSE abundances and the distribution of heat-producing elements within the crust and mantle. Several such models of the Earth's antineutrino flux[32,40,41] existed before the observation of geoneutrinos; with several recent models being presented with the inclusion of geoneutrinos[36,42,43]. All of the aforementioned models incorporate several geophysical models based on the crust and mantle from traditional geophysical measurements (seismology, chondritic meteorites, etc.) This effort, AGM2015, aims to consolidate all these models into a user-friendly interactive map, freely available to the general public and easily accessible to anyone with a simple web browser at http://www.ultralytics.com/agm2015.

Future work includes completing a more detailed uncertainty study using Monte Carlo methods. Such a study requires an accurate understanding of the uncertainty in each of the AGM elements listed in Tables 1 and 4, however, as well as the correlations that govern their interactions. Future geo-$\overline{\nu}_e$ measurements, updated flavor oscillation parameters, advances in crust/mantle models, and the ongoing construction and decommissioning of nuclear reactors around the world necessitates a dynamic AGM map capable of changing with the times. For this reason we envision the release of periodic updates to the original AGM2015, which will be labeled accordingly by the year of their release (i.e. "AGM2020").

Methods

AGM2015 uses CRUST1.0[35] to model the Earth's crustal density and volume profile via eight stratified layers. Elemental abundances for U, Th and K, and isotopic abundances for ^{238}U, ^{232}Th and ^{40}K for each layer were defined by Huang *et al.*[36]. These values were coupled to well known isotope half-lives and multiplicities to create $\overline{\nu}_e$ luminosities emanating from each crust tile. A similar approach was taken with the Earth's mantle, with elemental abundances derived via estimates of geo-$\overline{\nu}_e$ flux at KamLAND and Borexino[44] and density profiles supplied via PREM[39].

Man-made reactors were modeled via the IAEA PRIS[24] database, with reactor-$\overline{\nu}_e$ luminosities found to scale as $1.83 \times 10^{20} \overline{\nu}_e/\mathrm{s}/\mathrm{GW}_{\mathrm{th}}$. Reactor-$\overline{\nu}_e$ spectra were modeled as exponential falloffs from empirical data[19], while ^{238}U, ^{232}Th and ^{40}K spectra were modeled based on the work of Sanshiro Enomoto[37].

Luminosities from each point-source were converted to fluxes at each map location via the $P_{e \to e}$ survival probability shown in Equation (4), and a full understanding of the source spectra of each point-source enabled a complete reconstruction of the observed energy spectra at each map location. "Smart" integration was applied where necessary to more accurately portray crust and mantle tiles as volume-sources rather than point-sources. All modeling and visualization was done with MATLAB[45]. Google Maps and Google Earth multi-resolution raster pyramids created with MapTiler[46]. All online content available at http://www.ultralytics.com/agm2015.

References

1. Fermi, E. Versuch einer Theorie der β-Strahlen. *Zeitschrift für Physik*. **88,** 161–177 (1934).
2. Davis, Jr. R. Attempt to detect the antineutrinos from a nuclear reactor by the Cl^{37} ($\overline{\nu}_e$ e^-) Ar^{37} reaction. *Phys. Rev.* **97,** 766–767 (1955).

3. Cowan, Jr. C. L., Reines, F., Harrison, F. B., Kruse, H. W. & McGuire, A. D. Detection of the free neutrino: a confirmation. *Sci.* **124,** 103–104 (1956).
4. Reines F. & Cowan, Jr. C. L. The neutrino. *Nature*. **178,** 446–449 (1956).
5. Danby, G. T. *et al.* Observation of high-energy neutrino reactions and the existence of two kinds of neutrinos. *Phys. Rev. Lett.* **9,** 36–44 (1962).
6. Reines, F. *et al.* Evidence for high-energy cosmic-ray neutrino interactions. *Phys. Rev. Lett.* **15,** 429–433 (1965).
7. Achar, C. V. *et al.* Detection of muons produced by cosmic ray neutrinos deep underground. *Phys. Lett.* **18,** 196–199 (1965).
8. Haxton, W. C., Robertson, R. G. H. & Serenelli, A. M. Solar neutrinos: status and prospects. *ARA&A*. **51,** 21–61 (2013).
9. Hirata, K. *et al.* Observation of a neutrino burst from the supernova SN1987A. *Phys. Rev. Lett.* **58,** 1490 (1987).
10. Bionta, R. M. *et al.* Observation of a neutrino burst in coincidence with supernova 1987A in the Large Magellanic Cloud. *Phys. Rev. Lett.* **58,** 1494 (1987).
11. Alekseev, E. N. *et al.* Detection of the neutrino signal from SN 1987A in the LMC using the INR Baksan underground scintillation telescope. *Phys. Lett. B.* **205,** 209–214 (1988).
12. Gando, A. *et al.* Reactor on-off antineutrino measurement with KamLAND. *Phys. Rev. D*. **88,** 033001 (2013).
13. Bellini, G. *et al.* Measurement of geo-neutrinos from 1353 days of Borexino. *Phys. Lett. B*. **722,** 295–300 (2013).
14. Aartsen, M. G. *et al.* Evidence for high-energy extraterrestrial neutrinos at the IceCube detector. *Sci*. **22,** 6161 (2013).
15. Eder, G. Terrestrial neutrinos. *Nuclear Physics*. **78,** 657–662 (1966).
16. Kobayashi, M. & Fukao, Y. The earth as an antineutrino star. *Geophys. Res. Lett.* **18,** 633–636 (1991).
17. Grabas, H. *et al.* RF strip-line anodes for Psec large-area MCP-based photodetectors. *Nuc. Instrum. Meth. A*. **711,** 124–131 (2013).
18. Tanaka, H. K. M. & Watanabe, H. ^{6}Li-loaded directionally sensitive anti-neutrino detector for possible geo-neutrinographic imaging applications. *Sci. Rep.* **4,** 4708 (2014).
19. Bernstein, A. *et al.* Nuclear security applications of antineutrino detectors: current capabilities and future prospects. *Science & Global* **Security.18,** 3, 127–192 (2010).
20. Fogli, G. L., Lisi, E., Marrone, A., Montanino, D., Palazzo, A. & Rotunno, A. M. Global analysis of neutrino masses, mixings, and phases: Entering the era of leptonic CP violation searches. *Phys. Rev. D.* **86,** 013012 (2012).
21. An, F. P. *et al.* Observation of electron-antineutrino disappearance at Daya Bay. *Phys. Rev. Lett.* **112,** 061801 (2014).
22. Wolfenstein, L. Neutrino oscillations in matter. *Phys. Rev. D*. **17 (9)**, 2369 (1978).
23. Abazajian, K. N. *et al.* Light sterile neutrinos: a whitepaper. arXiv:1204.5379v1 (2012).
24. Mandula, J. Operating Experience with Nuclear Power Stations in Member States in 2013 2014 Edition, *IAEA*. **STI/PUB/1671** (2014).
25. Reboulleau, R., Lasserre, T. & Mention, G. Undeclared nuclear activity monitoring. Paper presented at The 6th International Workshop on Applied Anti-Neutrino Physics, Sendai, Japan. Tohuku University (2010, August 3).
26. Jocher, G. R. *et al.* Theoretical antineutrino detection, direction and ranging at long distances. *Phys. Rep*. **527,** 131–204 (2013).
27. McDonough, W. F. Compositional model for the Earths core, in Treatise on Geochemistry. vol. 2, *The Mantle and the Core*, edited by R. W., Carlson, H. D., Holland & K. K., Turekian, pp. 547–568 Elsevier, New York (2003).
28. Gomi, H. *et al.* The high conductivity of iron and thermal evolution of the Earths core. *Physics of the Earth and Planetary Interiors*. **224,** 88–103 (2013).
29. Lay, T., Hernlund, J. & Buffett, B. A. Core-mantle boundary heat flow. *Nature Geoscience*. **1,** 25–32 (2008).
30. Arevalo, R., McDonough W. F. & Luong, M. The K/U ratio of the silicate Earth: Insights into mantle composition, structure and thermal evolution. *Earth Planet. Sci. Lett.* **278(3-4),** 361–369 (2009).
31. Dye, S. T., Huang, Y., Lekic, V., McDonough, W. F. & Sramek, O. Geo-neutrinos and Earth Models. *Physics Procedia*. **61,** 310–318 (2015).
32. Mantovani, F., Carmignani, L., Fiorentini, G. & Lissia, M. Antineutrinos from earth: a reference model and its uncertainties. *Phys. Rev. D*. **69,** 01300 (2004).
33. Amante, C. & Eakins, B. W. ETOPO1 1 arc-minute global relief model: procedures, data sources and analysis. *NOAA Technical Memorandum NESDIS NGDC*. **24,** 19 (2009).
34. Pavlis, N. K., Holmes, S. A., Kenyon, S. C. & Factor, J. K. The development and evaluation of the earth gravitational model 2008 (EGM2008). *J. Geophys. Res.* **117,** B04406 (2012).
35. CRUST1.0 http://igppweb.ucsd.edu/gabi/crust1.html (Accessed: 20th November 2014).
36. Huang, Y., Chubakov, V., Mantovani, F., Rudnick, R. L. & McDonough, W. F. A reference Earth model for the heat-producing elements and associated geoneutrino flux. *Geochem. Geophys., Geosyst.* **14,** 6 (2013).
37. http://www.awa.tohoku.ac.jp/sanshiro/research/geoneutrino/spectrum/index.html (Accessed: 20th November 2014).
38. Dye, S. T. *et al.* Earth Radioactivity Measurements with a Deep Ocean Anti-neutrino Observatory. *Earth, Moon & Planets*. **99,** 241–252 (2006).
39. Dziewonski, A. M. & Anderson, D. L. Preliminary reference earth model. *Phys. Earth Planet. Int*. **25,** 297–356 (1981).
40. Enomoto, S., Ohtani, E., Inoue, K. & Suzuki, A. Neutrino geophysics with KamLAND and future prospects. arXiv:hep-ph/0508049 (2005).
41. Fogli, G. L., Lisi, E., Palazzo, A. & Rotunno, A. M. KamLAND neutrino spectra in energy and time. *Phys. Lett. B.* **623,** 80 (2005).
42. Fiorentini, G., Fogli, G., Lisi, E., Mantovani, F. & Rotunno, A. Mantle geoneutrinos in KamLAND and Borexino. *Phys. Rev. D.* **86,** 3 (2012).
43. Sramek, O., McDonough, W. F., Kite, E. S., Lekic, V., Dye, S. T. & Zhong, S. Geophysical and geochemical constraints on geoneutrino fluxes from Earth's mantle. *Earth Planet. Sci. Lett.* **361,** 356–366 (2013).
44. Ludhova, L. & Zavatarelli, S. Studying the Earth with Antineutrinos. *Adv. High Ener. Phys*. **2013,** 425693, doi: 10.1155/2013/425693 (2013).
45. MathWorks 2014, MATLAB ver. 2014b computer program, The MathWorks Inc., Natick, MA, USA.
46. MapTiler by Klokan Technologies GmbH, Hofnerstrasse 96, 6314 Unterageri, Switzerland, Europe http://www.maptiler.com (Accessed: 20th November 2014).
47. Kopeikin, V., Mikaelyan, L. & Sinev, V. Reactor as a source of antineutrinos: Thermal fission energy. *Phys. Atom. Nucl.* **67,** 1892–1899 (2004).
48. Begemann, F. *et al.* Towards and improved set of decay constants for geochronological use. *Geochim. Cosmochim Acta.* **65,** 111–121 (2001).
49. Blum, J. D. [Isotope Decay data] Global Earth physics: a handbook of physical constants [Ahrens, T. J. (ed.)] [271–282] (American Geophysical Union, Washington, DC) 1995.

Acknowledgements

We would like to thank S. Enomoto & M. Sakai for discussions at various phases of this project. This work is supported in part by a National Science Foundation grants EAR 1068097 and EAR 1067983, the U.S. Department of Energy, and the National Geospatial-Intelligence Agency.

Author Contributions

S.M.U. suggested this study. G.R.J. conducted all simulations and incorporated models written by S.D., W.F.M. and J.G.L. Mapping formats and standards were developed by G.R.J. and S.M.U. All authors contributed to writing the paper.

Additional Information

Competing financial interests: The authors declare no competing financial interests.

How to cite this article: Usman, S.M. *et al.* AGM2015: Antineutrino Global Map 2015. *Sci. Rep.* **5**, 13945; doi: 10.1038/srep13945 (2015).